Synthesis of Nanocrystalline Zirconium Titanate and its Dielectric Properties

S. V. Pol,[†] V. G. Pol,[†] A. Gedanken,*[,†] G. I. Spijksma,[§,||] J. Grinblat,[†] R. Kalai Selvan,[‡] V. G. Kessler,[§] G. A. Seisenbaeva,[§] and S. Gohil[§]

Department of Chemistry and Kanbar Laboratory for Nanomaterials at the Bar-Ilan University Center for Advanced Materials and Nanotechnology, Bar-Ilan University, Ramat-Gan 52900, Israel, Central Electrochemical Research Institute, Karaikudi-630 006, India, Department of Chemistry, SLU, Swedish University of Agricultural Sciences, Box 7015, 75007 Uppsala, Sweden, and Inorganic Materials Science, University of Twente & MESA+ Institute for Nanotechnology, P.O. Box 217, 7500 AE Enschede, The Netherlands

Received: October 30, 2006; In Final Form: December 17, 2006

The thermal decomposition of a $ZrTi_2[(OC_2H_4)_2NH]_3(OC_3H_7)_6$ precursor by the RAPET (reaction under autogenic pressure at elevated temperature) method provided the formation of crystalline zirconium titanate nanoparticles. These as-prepared nanoparticles are embedded in a carbon shell, which can be removed completely by calcination at 500 °C under air for 3 h, resulting in pure white crystalline nanoparticles. At a reaction temperature of 700 °C, the nanoparticles are mainly $ZrTi_2O_6$ (srilankite), whereas at 800 °C, the product is predominately $Zr_5Ti_7O_{24}$. The structural, morphological, compositional, magnetic, and AC electrical properties are measured for the as-prepared $ZrTi_2O_6$ embedded in carbon (ZTEC), as well as the crystalline $ZrTi_2O_6$ nanoparticles (ZTN) obtained after sintering. The reaction mechanism is based on the decomposition products containing pyrrol and pyrazine. The presence of these compounds provides an understanding of the decomposition of the diethanolamine ligands and the formation of the nanoparticles in general.

Introduction

Zirconium titanate (ZT)-based ceramic materials have many attractive properties: high resistivity, high dielectric constant, high permittivity at microwave frequencies, and excellent temperature stability for microwave properties.[1,2] These materials have an extremely wide range of application, such as in microwave telecommunications (as capacitors, dielectric resonators in filters, and oscillators) and in catalysis (as effective acid−base bifunctional catalysts and photocatalysts).[3,4] As is true for many other materials, the ultrafine-grained, high-quality powders of ZT are in great demand. Fine powders are necessary precursors for making monolithic ceramics via casting, as well as ceramic films via a coating process. For such a binary (two-metal elements) oxide system, compositional homogeneity and microstructure uniformity (low or no phase segregation) are very important. It is well-known that powder characteristics (such as particle size, shape, size distribution, agglomeration, crystallite size, and chemical and phase composition) determine to a large extent the microstructures developed during sintering and thus affect the properties of ceramic materials.[5,6] $ZrTiO_4$ and $ZrTi_2O_6$ (srilankite) both have orthorhombic crystal structures and similar diffraction lines.

Various solution-based wet chemical syntheses have been developed as alternatives to the conventional solid-state-reaction route in order to obtain high-purity and more homogeneous zirconium titanate materials. The solid-state reaction normally requires high temperatures (1200−1700 °C) over a prolonged period for the homogeneous materials' synthesis from the mixed crystalline ceramic oxides, ZrO_2 and TiO_2,[7,8] and also requires posttreatment such as energy-intensive grinding/milling procedures for powder formation. However, this process usually leads to inhomogeneous, coarse, and multiphase powders of poor purity.[9] Several major wet-chemical routes have been studied for the synthesis of ZT materials and include the following: (1) Classical hydrolytic sol−gel procedures, where metal alkoxides are dissolved in alcohol in order to prepare a precursor gel, which is then dried, calcined, and ground to a fine powder.[10−12] (2) Ikawa et al.[13] achieved the coprecipitation of $Zr(SO_4)_2$ and $Ti(SO_4)_2$ using concentrated aqueous ammonia. (3) Leoni et al.[1] produced ZT nanopowders by the chemical precipitation of an aqueous solution of $TiCl_4$ and $ZrOCl_2$ using ammonia. (4) Stubicar et al.[14] synthesized $ZrTiO_4$ oxide powder by ball milling an equal molar powder mixture of ZrO_2-TiO_2 and postanneal processing. A fully amorphous structure appeared during ball milling and required further thermal processing for crystallization. (5) Micrometer spheres of zirconium titanate were produced by homogeneous dielectric-tuning coprecipitation.[15] (6) Long $ZrTiO_4$ fibers have been synthesized through a sol−gel process using titanium sulfate and zirconium oxychloride octahydrate as starting materials without any organic component.[16] (7) Bianco et al. also reported on a polymeric precursor route to synthesize zirconium titanate microwave dielectrics.[2] Zirconiumdititanate, $ZrTi_2O_6$, commonly referred to as srilankite[17] and considered as difficult to prepare, is found in nature as a volcanic mineral and could earlier be obtained only by applying a very high pressure (28 kBar) and temperature (1500 °C).[18] Srilankite is of great interest as a dielectric material, but its application has been hindered by the difficulty in its synthesis[19] (requires high pressures and temperatures). Recently, the synthetic method with flux and seeds developed[20a] for high pressures was successfully applied to syntheses at atmospheric

* Corresponding author. E-mail: gedanken@mail.biu.ac.il.
† Bar-Ilan University.
‡ Central Electrochemical Research Institute.
§ SLU, Swedish University of Agricultural Sciences.
|| University of Twente & MESA+ Institute for Nanotechnology.

10.1021/jp067109z CCC: $37.00
Published on Web 01/24/2007

pressure, and effectively equilibrated the phase assemblages in the ZrO_2-TiO_2 system below 1200 °C. Additionally, microporous zirconia-titania composite membranes have been fabricated by sol−gel processing[20b] using diethanolamine-modified precursor solutions.

In this article, we report on the facile rapid synthesis of $ZrTi_2O_6$ (srilankite) embedded in carbon by the thermal decomposition of a $ZrTi_2[(OC_2H_4)_2NH]_3(OC_3H_7)_6$ precursor at a relatively low temperature (700 °C) in a closed Swagelok cell. The reaction mechanism is elucidated by collecting and isolating organic volatiles after the decomposition of a $ZrTi_2[(OC_2H_4)_2NH]_3(OC_3H_7)_6$ precursor using the GC-MS technique. The pure white nanocrystalline $ZrTi_2O_6$ is obtained after sintering $ZrTi_2O_6$ embedded in carbon at 500 °C under air for 3 h. The present nonaqueous, solvent-, catalyst-, and template-free single-precursor reaction opens a facile route to synthesize uncommon $ZrTi_2O_6$ nanocrystals at relatively low temperatures, which can be up scaled. The structural, morphological, compositional, magnetic, and AC electrical properties are measured for the as-prepared $ZrTi_2O_6$ embedded in carbon, as well as the $ZrTi_2O_6$ nanocrystals obtained after sintering. Earlier, such a one-stage, efficient, and uncomplicated economic RAPET technique was employed for the fabrication of various interesting nanostructures.[21−22] The main difference between our previous RAPET studies and the current one is as follows: previously, we utilized a pure metal (single) alkoxide or metal acetyl acetonate precursors possessing only H, C, and O elements in the ligands. These reactions yielded a metal oxide core and carbon as a shell. Thus, it is interesting to evaluate the action of two metals with the nitrogen-containing diethanolamine ligands during the thermal decomposition of the $ZrTi_2[(OC_2H_4)_2NH]_3(OC_3H_7)_6$ precursor.

Experimental Section

(1) Synthesis of a $ZrTi_2[(OC_2H_4)_2NH]_3(OC_3H_7)_6$ Precursor. A total of 0.57 g (1.5 mmol) of zirconium isopropoxide was dissolved in a 3 mL mixture of hexane/toluene (volume ratio 2:1), after which 0.84 g (∼3.0 mmol) of titanium isopropoxide and 0.46 g (∼4.4 mmol) of diethanolamine (H2dea) (98%, Aldrich) were added. The sample was dried under vacuum (0.1 mmHg) and redissolved in 2 mL of hexane. After cooling overnight in a freezer at −30 °C, the obtained colorless octahedral crystals were separated from the solvent by decantation. The yield of the product was ∼1.1 g (∼59%).

Samples of crystals of **1** were dried in vacuum (0.1 mmHg) for 2 h prior to spectral studies and microanalysis. Found (%): C 41.8; N 5.0; H 7.5. Calculated for $C_{30}H_{69}N_3O_{12}Ti_2Zr$ (%): C 42.3; N 4.9; H 8.1. The IR spectra were recorded of the compound in nujol mulls, cm^{-1}: 1358 sh, 1327 w, 1280 w, 1241 w, 1167 sh, 1160 m, 1124 s, 1085 m, 1060s, 1007 w, 988 s, 941 m, 914 s, 879 m, 844 s, 673 sh, 602 s, 571 sh, 447 s. The molecular structure of this compound, determined[23] earlier by us, is displayed in Scheme 1.

(2) Fabrication of Nanocrystalline ZTN Embedded in Carbon and Its Conversion to $ZrTi_2O_6$ Nanoparticles. The fabrication of nanocrystalline $ZrTi_2O_6$ embedded in carbon (ZTEC) was carried out by introducing the $ZrTi_2[(OC_2H_4)_2NH]_3(OC_3H_7)_6$ precursor into a 3 mL closed cell. The cell was assembled from stainless steel Swagelok parts. A 1/2″ union part was capped on both sides by standard plugs. For this synthesis, 1.5 g of the above precursor was introduced into the cell at room temperature in a nitrogen-filled glove box. The filled cell was closed tightly by the other plug and then placed inside an iron pipe in the middle of the furnace. The temperature was raised at a heating rate of 25 °C per minute. The closed

SCHEME 1: Diagram Showing the Molecular Structure of the $ZrTi_2(OC_2H_4)_6N_3H_3(OC_3H_7)_6$ Precursor

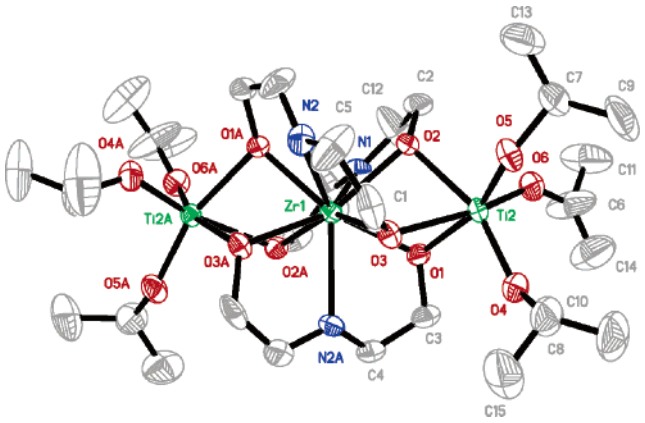

vessel cell was heated at 700 °C for 1 h. The reaction took place under the autogenic pressure of the precursor. The Swagelok was gradually cooled (∼5 h) to room temperature and opened, and a black powder was obtained. The total yield of the product material was 56% of the total weight of the materials introduced into the cell (the yield was the final weight of the product relative to the weight of $ZrTi_2[(OC_2H_4)_2NH]_3(OC_3H_7)_6$, the starting material). The present synthesis of nanocrystalline $ZrTi_2O_6$ embedded in carbon via the RAPET method required the use of simple equipment reported elsewhere,[24] a comparatively low temperature, and a short reaction time. There is no effect on the crystalline nature and morphology of the product when the reaction time is changed from 1 to 3 h. The as-prepared nanocomposite $ZrTi_2O_6$ embedded in carbon was further annealed at 500 °C under air, yielding white $ZrTi_2O_6$ nanoparticles (ZTN). The 35% weight loss observed was due to the loss of carbon (while annealing). The CHNS analysis also measured ∼36 wt % of carbon in ZTEC product. Therefore, the calculated weight of Zr and Ti metals in the precursor and the product are accounted. The Zr (160.95 mg) and Ti (168.90 mg) are calculated in 1.5 g of precursor, which resulted in Zr (173.32 mg) and Ti (181.92 mg) in the 840 mg of ZTEC product. The weight of Zr and Ti metals is observed to be a bit higher than in the reactant due to the variation in obtained carbon %. The measured BET surface areas of the ZTEC and ZTN are 42.2 and 53.5 m^2/g, respectively.

(3) Characterizations. The X-ray diffraction pattern of the products was measured with a Bruker AXS D* Advance Powder X-ray diffractometer (using Cu Kα = 1.5418 Å radiation). Elemental analysis of the ZTEC and ZTN was carried out on an Eager 200 C,H,N,S analyzer. The elemental composition of the materials and the SEM image were analyzed by energy-dispersive X-ray (EDX) analysis on a JEOL-JSM 840 scanning electron microscope. The particle morphology and structure were studied using transmission electron microscopy (TEM) on a JEOL-JEM 100 SX microscope (80 kV accelerating voltage) and a JEOL-2010 HRTEM instrument (200 kV accelerating voltage). The TEM and HR-TEM samples were prepared by ultrasonically dispersing the products into absolute ethanol and subsequently placing a drop or two of this suspension onto a copper grid coated with an amorphous carbon film, and then drying under air. A Micromeritics (Gemini 2375) surface area analyzer was used to measure the surface area of the ZTEC and ZTN samples.

The AC electrical conductivity of the studied materials was carried out using a computer controlled HIOKI 3532 LCR Meter. The measurements were conducted at room temperature

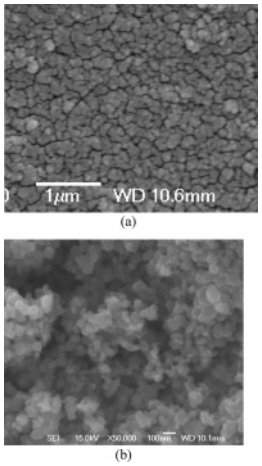

Figure 1. (a) ZTEC sample and (b) ZTN sample.

over a frequency range of 42 Hz to 5 MHz. The powders were compacted with the addition of PVDF binder in 1 cm diameter and 0.3 cm thickness pellets by using a hydraulic press applying 3.5 tons /cm^2. Then the pellets were sintered at 150 °C for 2 h. The silver paint was coated on both sides of the pellet to act as a blocking electrode and also to provide the mechanical strength.

The following experiments were conducted for the elucidation of the decomposition mechanism of the precursor. The $ZrTi_2[(OC_2H_4)_2NH]_3(OC_3H_7)_6$ precursor (~0.5 g) was placed in an evacuated (10^{-2} mmHg) glass vessel with a total volume of 25 mL and quickly warmed up to 500 °C. After being kept at this temperature for 10 min, it was connected via a short glass tube to another evacuated glass vessel cooled by liquid nitrogen. The organic volatiles were collected and isolated by the GC-MS technique using a Hewlett-Packard 5890 Series II gas chromatograph supplied with a capillary separating column with a DB-Wax film phase (manufactured by J&W Scientific, CA) and coupled with a Jeol JMS-SX/SX102A tandem mass spectrometer.

Results and Discussion

The morphology of the obtained powders (labeled ZTEC and ZTN, referring to the uncalcined and the calcined sample, respectively) is investigated by scanning electron microscopy (SEM). Agglomerates of metal oxides with a diameter around 150 nm embedded in carbon are observed (Figure 1a). The sintering of ZTEC at 500 °C under air for 3 h led to the removal of the carbon and provided particles with a diameter of <100 nm [Figure 1b]. The description of the particle size determination is outlined in the following TEM section.

It is interesting to evaluate the role of the nitrogen containing diethanolamine ligands during decomposition. We have calculated the element (wt) percent of carbon, hydrogen, oxygen and nitrogen in the precursor $[ZrTi_2[(OC_2H_4)_2NH]_3(OC_3H_7)_6]$ and compared it with the obtained elemental analysis data examined by an elemental analyzer. The calculated element percent of carbon in the precursor was 43% (in 1.5 grams of the precursor), the percentage of hydrogen was 6.8%, and that of nitrogen was 3.4%. The measured element percentage of carbon in the ZTEC product was 36.3% (in 0.84 grams of the product), the percentage of hydrogen was 0.2%, and the amount of nitrogen was negligible. The measured element percentage of carbon and hydrogen in the ZTN was 0.6 and 0.1% (wt), respectively. It is remarkable that there is no nitrogen in the core or shell, and hence, it can be expected that the diethanolamine decomposes to volatile compounds.

The decomposition mechanism of the diethanolamine was further investigated by the thermal decomposition of the precursor and the subsequent collection of the released volatiles. The isolated organic volatiles consist of three major types of constituents: highly volatile components, isopropanol and water, components with low volatility involving four major fractions identified as pyrrol, pyrazine, methyl-pyrazine and dimethyl-pyrazine, and, finally, a polymeric nitrogen-containing residue which was not volatile under experimental conditions (evaporator temperature, 180 °C). Pyrrols and pyrazines are known as typical products of the thermal decomposition of α-aminoacids (proteins) in a non-oxidative atmosphere (reductive cyclization).[25−27a] Their formation is facilitated by the presence of polyols, for example, sugars and protic catalysts. The decomposition of a diethanolamine-modified alkoxide follows most probably this type of condensation. The diethanolamine unit is already a reduced species, containing an ethylene fragment that is necessary for the realization of a 6-member heterocycle.

The zirconium titanate nanoparticles are most probably initially formed through quick high-temperature hydrolysis of the precursor by water released through dehydration of isopropanol in the primary steps of decomposition. The metal oxides play the role of a protic catalyst and facilitate the reactions of dehydration and dehydrogenation and also lead to the polymerization of the unsaturated organic fragments.[27b] These organic fragments result finally in the formation of amorphous carbon shells around the metal oxide core.

The morphology of the ZTEC sample is further studied by transmission electron microscopy (TEM). Figure 2a displays spherical particles surrounded by a layer of contrasting material. The diameter of these dark cores (marked with white circles) ranges between 12 and 25 nm (Figure 2a). The higher magnification image on a single particle displays disordered lattice planes of carbon (Figure 2b) around the dark ziconium-titanate core. These disordered layers correspond to the non-graphitic, coal-like lattice planes of the carbon, which were not detected in XRD measurements (discussed below). The interlayer spacing is ~3.74 Å, which is slightly larger than that of the graphite layers. The HR-TEM image also reveals that the core of the particle is a nanocrystalline material with a perfect defect-free arrangement of the atomic layers. The measured distance between these (111) lattice planes is 0.291 nm. This value is very close to that of both $ZrTi_2O_6$ [PDF No. 46−1265] and $ZrTiO_4$ [PDF No. 34−0415], whose values are 0.290 and 0.293 nm, respectively.

The ZTEC sample was calcined at 500 °C under air to burn off the carbon. The calcination process led to a slight increase in the particle size to 25−50 nm (Figure 2c). The HR-TEM image depicted in Figure 2d illustrates again the perfect defect-free arrangement of the atomic layers of several particles lying on various planes. The highlighted distance between these (110) lattice planes is 0.353 nm. This value is very close to the distance between the planes reported in the literature (0.35 nm) for the orthorhombic lattice of $ZrTi_2O_6$ [PDF No. 46−1265]. The interlayer spacing of $ZrTiO_4$ that is closest to the observed distance is 0.362 nm of the (011) lattice plane. Thus, the composition of the crystalline nanoparticles is most probably $ZrTi_2O_6$, based on the lattice distances of perfectly arranged atomic layers of the particles. In addition, the EDX analysis provided a Zr/Ti element ratio of 1:2.01, which is in agreement with the expected ratio of $ZrTi_2O_6$.

The electron diffraction (ED) patterns of the ZTEC and ZTN particles, displayed as inserts in panels b and d of Figure 2, respectively, are in good agreement with those expected for $ZrTi_2O_6$. The ED pattern of the ZTEC particles (Figure 2b) can

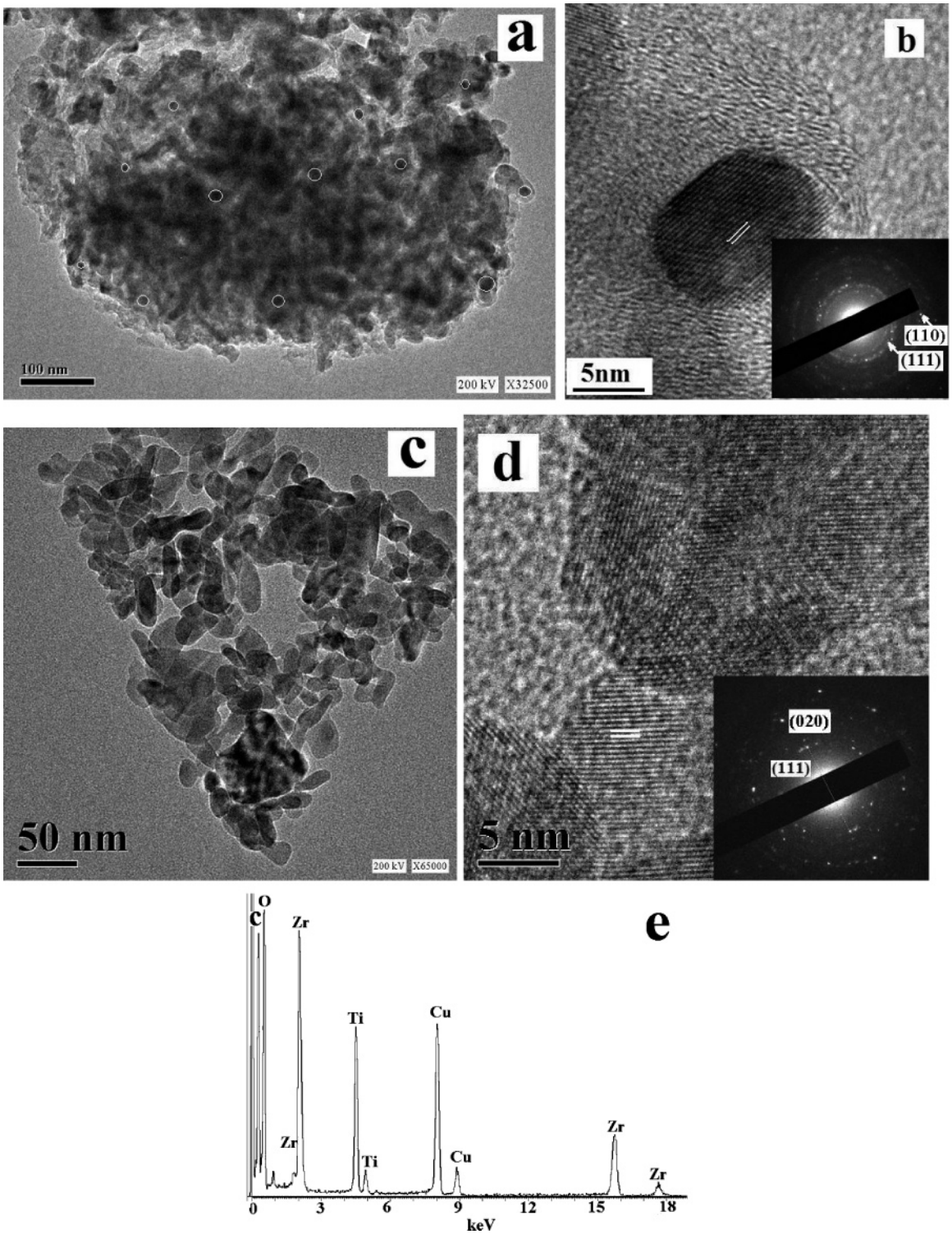

Figure 2. (a) ZTEC sample, (b) HR-TEM ZTEC sample, (c) ZTN sample, (d) HR-TEM of ZTN sample, and (e) SAEDS of ZTEC sample.

be indexed to the reflection of the (110) and (111) planes and that of the ZTN particles to the (111) and (020) planes.

The representative SAEDS of the ZTEC sample was obtained by focusing a 35 nm electron beam on the ZTEC particles [Figure 2e]. The presence of Zr, Ti, O, C, and Cu is observed. The Cu signal originates from the TEM grid.

X-ray diffraction was performed on the ZTEC and ZTN samples. The diffractograms of both samples are very similar and display broad signals as a result of the nanosize dimension of the material. In the ZTEC sample, there is no clear diffraction peak for graphitic carbon at $2\theta = 26.6°$, which might be due to the formation of disordered carbon at low temperature (700 °C). There is an increase in the intensity and a decrease in the fwhm of all of the peaks observed in the ZTN sample (Figure 3a). The position of the most intense peak in the diffractograms of both materials is around $2\theta = 30.7°$. At this position, the most intense peak is found for tetragonal zirconia and for zirconium-titanates. However, the other strong signals due to zirconia are not present. In addition, for the presence of bare zirconium, a large amount of the titania phase should be observed since the EDX and the original precursor displayed Zr and Ti in a ratio of 1:2. The most intense peak of anatase would be around 2θ

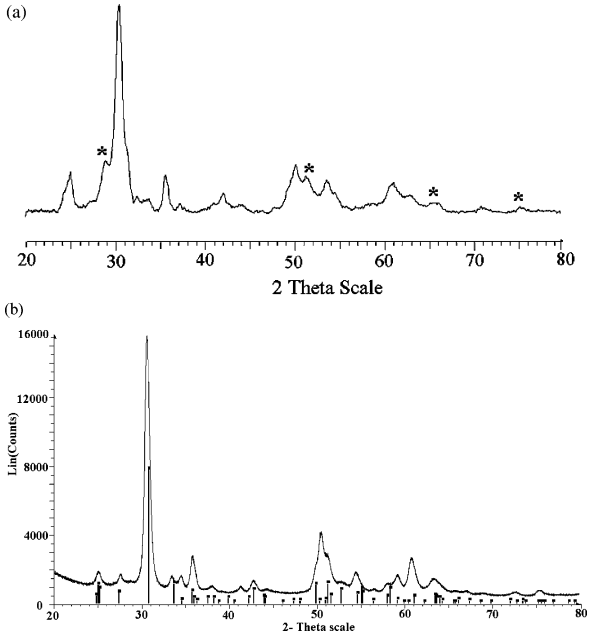

Figure 3. (a) Powder XRD patterns of the zirconium-titanate sample prepared at 700 °C, (a) followed by calcination (500 °C in air) and (b) a zircoinum titanate sample prepared at 800 °C.

$= 25.5°$. The observed peak around this angle does not have the intensity that would assign the peak at $2\theta = 30.5°$ to zirconia. The other strong signals (at 50.1 and 60.5° 2θ) are also very weak. For the same reason (i.e., a not intense enough signal from titania), it is unlikely that the most intense peak is due to $ZrTiO_4$ [PDF No. 34−0415]. Therefore, the major phase present in the samples is $ZrTi_2O_6$ [PDF No. 46−1265] with little contamination of tetragonal zirconia and anatase titania (peaks marked by stars).

The Scherrer equation is used to calculate the particle dimensions,[28] and an average particle size of ∼20 nm is calculated for the ZTN sample considering the main peak at $2\theta = 30.7°$. The observed particle diameter is in agreement with the TEM measurements (Figure 2a).

An additional RAPET experiment was performed at 800 °C in order to verify the temperature effect on the phase composition. The XRD pattern of the obtained product is depicted in Figure 3b. The peak positions and intensities match very well with the orthorhombic $Zr_5Ti_7O_{24}$ phase [34−0209]. A similar XRD pattern was obtained for the sample after the removal of carbon by burning. The fwhm of all of the peaks became narrower. This is analogous to the sample prepared at 700 °C (described above) and probably due to the growth of the particles during the heat treatment. Thus, it seems that the composition is dependent on the synthesis temperature. Further optimization of the synthesis conditions should allow for the future preparation of single phase materials. Regardless of the impurities in the sample prepared at 700 °C, it is interesting to determine its properties as its nanosized dimension makes the material unique.

The electron paramagnetic resonance (EPR) spectra of the ZTEC and ZTN samples were measured at room temperature and a representative EPR is shown in Figure 4 for ZTEC. The *g*-factor is a dimensionless constant and is equal to 2.002319 for an unbound electron.[29] The intensity of the EPR signal in the ZTEC sample is 20 times stronger than the signal of the ZTN sample. The measured *g*-factors for the ZTEC and ZTN samples are 2.007 and 2.0031, respectively. The ZTEC showed a peak-to-peak separation (ΔH_{pp}) of ∼49 G, and a peak-to-peak separation of 42 G was determined for the ZTN sample. These narrow paramagnetic[30] resonance signals (width ∼45 G)

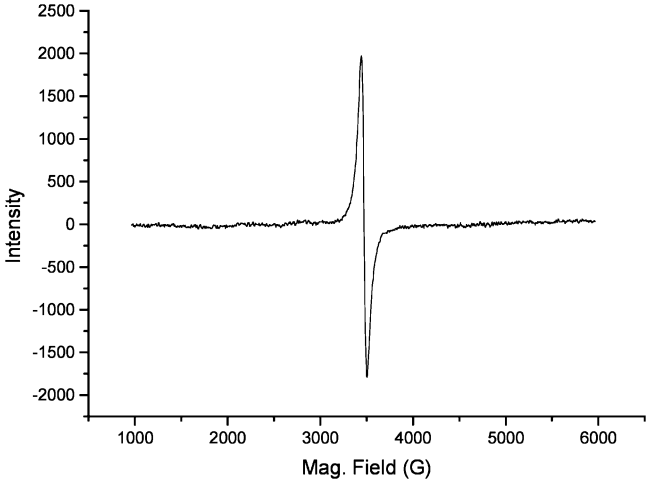

Figure 4. Representative EPR signal of ZTEC sample.

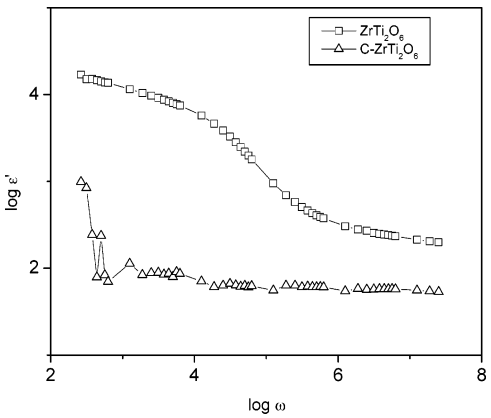

Figure 5. Dielectric constant vs frequency.

match the signal produced by nongraphitized carbon black. The crystalline $ZrTi_2O_6$ nanoparticle [ZTN] sample also showed an unusual EPR signal, interestingly. This signal might have originated from the carbon traces (<0.6%, confirmed by C, H, N, and S analysis) left in the ZTN sample after calcining the ZTEC sample.

The variation in a dielectric constant (ϵ') as a function of frequency [Figure 5] ranging from 42 Hz to 5 MHz for ZTN and ZTEC is noticed at ambient temperature. The decrease in dielectric constant with increasing frequency is recorded. The high value of a dielectric constant was observed for $ZrTi_2O_6$ samples due to the inhomogeneous structure of the materials, arising from the high-temperature calcination. Here, the high conducting grains are separated from low conducting grain boundaries, which act as a parallel combination of capacitance and resistance.[31] The observed normal dielectric behavior (i.e., the decrease in the dielectric constant with increasing frequency) is attributed to Maxwell−Wagner interfacial polarization[32] and substantiated by the Koops phenomenological theory.[33] The nanoparticles show a high volume fraction, and hence the interfacial polarization is dominant, which enhances the more dielectric behavior of $ZrTi_2O_6$. The $ZrTi_2O_6$ embedded in the carbon sample give the lower dielectric values, which confirm that the embedded particles are uniform and homogeneous in nature because of less particle agglomeration.

The conducting mechanism is confirmed by impedance measurements of the $ZrTi_2O_6$ sample (Figure 6). The results show only one semicircle, indicating the electrical process of the compound, which is mainly due to the contribution from bulk materials (grain interior) and which can be attributed to the parallel combination of capacitance and resistance. The

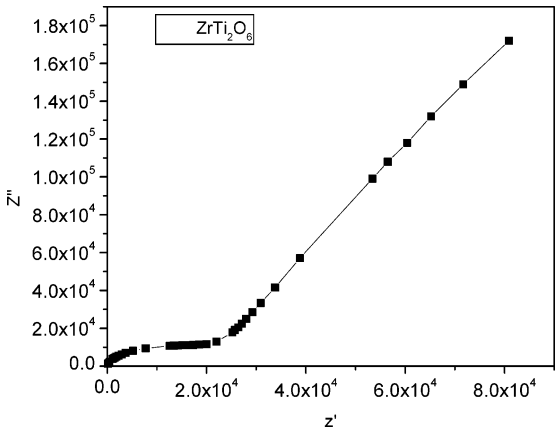

Figure 6. Impedance spectra of $ZrTi_2O_6$.

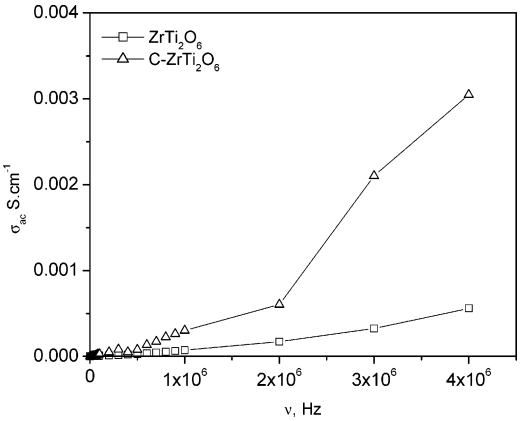

Figure 7. AC Conductivity vs frequency.

spectra also confirm the complete absence of a grain boundary effect, which also suggests that the principal charge carriers in these materials are the electrons or oxygen vacuum vacancies.[34]

Figure 7 shows the frequency-dependent AC electrical conductivity of ZTN and ZTEC measured at room temperature. As the frequency increases, the conductivity values increases, which reveals that the applied frequency enhances the hopping frequency, as well as the mobility of charge carriers. The observed two regions of (i) low frequency (frequency independent behavior) and (ii) high frequency (frequency dependent behavior) may be explained by Joncher's power law, $\sigma'(f) = \sigma_{dc}\,[1 + (f/f_p)^n]$, where σ_{dc} is the DC conductivity, f and f_p are applied frequency and relaxation frequency, and n is exponential, which is <1 for disordered solids.

At a low frequency (below f_p), the charge transport takes place on an infinite path, and hence the conductivity is minimum which corresponds to the DC conductivity.[35] At a higher frequency region, the conductivity is dominated by a hopping mechanism and obeys the power law resulting in an increase in the conductivity. The rate of increasing conductivity is large for ZTEC and also gives a higher conductivity of 3.04×10^{-3} $S.cm^{-1}$ because of the larger grain size (~30 nm) compared with the ZTN. If the grain size is reduced to a few nm, the grain boundary effect is dominant due to the large number of grains. In our case, though, a larger grain size is observed for ZTEC, which reduces the grain boundary effect and in turn enhances the conductivity.[35,36]

In conclusion, a nonaqueous, template-, surfactant−solvent-free approach was developed for the synthesis of dielectric $ZrTi_2O_6$ nanocrystals encapsulated in carbon, using a single precursor. Further annealing of the as-prepared $ZrTi_2O_6$ nanocrystals encapsulated in carbon at 500 °C for 3 h in air led to the formation of $ZrTi_2O_6$ nanoparticles. From the impedance spectra, the grain effect was predominant for the conducting mechanism of $ZrTi_2O_6$. The maximum AC conductivity was observed for $ZrTi_2O_6$-embedded carbon nanoparticles due to the absence of a grain boundary effect. The reaction mechanism is based on the decomposition products containing pyrrol and pyrazine.

References and Notes

(1) Leoni, M.; Viviani, M.; Battilana, G.; Fiprello, A. M.; Vitticoli, M. *J. Eur. Ceram. Soc.* **2001**, *21*, 1739.
(2) Bianco, A.; Gusmano, G.; Freer, R.; Smith, P. *J. Eur. Ceram. Soc.* **1999**, *19*, 959.
(3) Navio, J. A.; Colon, G. *New Dev. Selective Oxid. II* **1994**, *82*, 721.
(4) Navio, J. A.; Marchena, F. J.; Macias, M.; Sanchez-Soto, P. J.; Pichat, P. *J. Therm. Anal.* **1993**, *40*, 1095.
(5) Ellis, S. K.; Mcnamara, E. P. *J. Ceram. Bull.* **1989**, *68*, 988.
(6) Montanaro, L.; Guilhot, B. *J. Ceram. Bull.* **1989**, *68*, 1017.
(7) Azough, F.; Freer, R.; Wang, C. -L.; Lorimer, G. W. *J. Mater. Sci.* **1996**, *31*, 2539.
(8) Navio, J. A.; Macias, M.; Sanchez-Soto, P. J. *J. Mater. Sci. Lett.* **1992**, *11*, 1570.
(9) Xu, J.; Lind, C.; Wilkinson, A. P.; Pattanaik, S. *Chem. Mater.* **2000**, *12*, 3347.
(10) Hirano, S.; Hayashi, T.; Hattori, A. *J. Am. Ceram. Soc.* **1991**, *74*, 1320.
(11) Komarneni, S.; Abothu, I. R.; Rao, A. V. P. *J. Sol-Gel Sci. Technol.* **1999**, *15*, 263.
(12) Karakchiev, L. G.; Zima, T. M.; Lyakhov, N. Z. *Inorg. Mater.* **2001**, *37*, 386.
(13) Ikawa, H.; Yamada, T.; Kojima K.; Matsumoto, S. *J. Am. Ceram. Soc.* **1991**, *74*, 1459.
(14) Stubicar, M.; Bamanec, V.; Stubicar, N.; Kudrnovski, D.; Krumes, D. *J. Alloys Compd.* **2001**, *316*, 316.
(15) Hu, M. Z.-C.; Payzant, E. A.; Booth, K. R.; Rawn, C. J.; Hunt, R. D.; Allard, L. F. *J. Mater. Sci.* **2003**, *38*, 3831.
(16) Lu, Q.; Chen, D.; Jiao, X. *J. Mater. Chem.* **2003**, *13*, 1127.
(17) Willgallis, A.; Harti, H. *Z. Kristallogr.* **1983**, *164*, 59.
(18) Troitzsch, U.; Ellis, D. J. *Eur. J. Minerol.* **2004**, *16*, 577.
(19) Köstlin, H.; Frank, G.; Hebbinghaus, G.; Auding, H.; Denissen, K. *J. Non-Cryst. Solids* **1997**, *218*, 347.
(20) (a) Troitzsch, U.; Ellis, D. J. *J. Mater. Sci.* **2005**, *40*, 4572. (b) Spijksma, G. I.; Huiskes, C.; Benes, N. E.; Kruidhof, H.; Blank, D. H. A. Kessler, V. G.; Bouwmeester, H. J. M. *Adv. Mater.* **2006**, *18*, 2165.
(21) (a) Pol, V. G.; Pol, S. V.; Gedanken, A. *J. Phys. Chem. B* **2005**, *108*, 6121. (b) Pol, S. V.; Pol, V. G.; Frydman, A.; Churilov, G. N.; Gedanken, A. *J. Phys. Chem. B* **2005**, *109*, 9495. (c) Pol, S. V.; Pol, V. G.; Kessler, V. G.; Seisenbaeva, G. A.; Sung, M.; Asai, S.; Gedanken, A. *J. Phys. Chem. B* **2004**, *108*, 6322.
(22) (a) Pol, S. V.; Pol, V. G.; Seisenbaeva, G.; Kessler, V. G.; Gedanken, A. *Chem. Mater.* **2004**, *16*, 1793. (b) Pol, V. G.; Pol, S. V.; Gedanken, A. *Chem. Mater.* **2005**, *17*, 1797. (c) Pol, S. V.; Pol, V. G.; Gedanken, A.; Goffer, Y. *J. Mater. Chem.* **2004**, *14*, 966. (d) Pol, S. V.; Pol, V. G.; Kessler, V. G.; Seisenbaeva, G. A.; Solovyov, L. A.; Gedanken, A. *Inorg. Chem.* **2005**, *44*, 9938.
(23) Spijksma G. I.; Bouwmeester H. J. M.; Blank D. H. A.; Kessler V. G. *Inorg. Chem. Comm.* **2004**, *7*, 953.
(24) Pol, S. V.; Pol, V. G.; Gedanken, A. *Chem. Eur. J.* **2004**, *10*, 4467.
(25) Shu, C.-K. *J. Agric. Food Chem.* **1999**, *47*, 4332.
(26) Knerr Lerche, T.; Pischetsrieder, H.; Severin, T. *J. Agric. Food Chem.* **2001**, *49*, 1966.
(27) (a) McNab, H.; Morrow, M. *ARKAT* **2002**, *8*, 509. (b) Pol, S. V.; Pol V. G.; Kessler V. G.; Gedanken A. *New J. Chem.* **2006**, *30*, 370.
(28) Alexander, L. *X-Ray Diffraction Procedures*; Klug, H. Ed.; Wiley: New York, 1962; p 125.
(29) Willard, H. H.; Merrit, L. L.; Dean, J. A. *Instrumental Methods of Analysis*, 5th ed.; Van Nostrand: New York, 1974; p 236.
(30) (a) Pol, V. G.; Motiei, M.; Gedanken, A.; Calderon-Moreno, J. M.; Yoshimura, M. *Carbon* **2004**, *42*, 111. (b) Pol, V. G.; Pol, S. V.; Gedanken, A.; Sung, M-G.; Shigeo, A. *Carbon* **2004**, *42*, 2738.
(31) Bhattacharyya, S.; Krupanidhi, S. B. *J. Appl. Phys.* **2003**, *94*, 5135.
(32) Maxwell, J. C. *A treatise on Electricity and Magnetism*; Oxford University Press: Oxford, U.K., 1954; Vol. 2, Section 328.
(33) Koops, C. G. *Phys. Rev.* **1951**, *83*, 121.
(34) Kumar, A.; Singh, B. P.; Choudhary, R. N. P.; Thakur, A. K. *J. Alloys Compd.* **2005**, *394*, 292.
(35) Thangadurai, V.; Weppner, W. *J. Solid State Chem.* **2006**, *179*, 974.
(36) Selvan, R. Kalai; Kalaiselvi, N.; Augustin, C. O.; Doh, C. H.; *Electrochem. Solid State Lett.* **2006**, *9*, 390.